IMECE2020-23829

MODELING AND DESIGN OPTIMIZATION OF ROBOTIC HOSES FOR 3D PRINTING OF CEMENT

Peter Sterckx
Continuum Robotics Laboratory
Department of Mechanical Engineering
Clemson University
Clemson, South Carolina 29634
Email: psterck@clemson.edu

Ian D. Walker
Continuum Robotics Laboratory
Department of Electrical and Computer Engineering
Clemson University
Clemson, South Carolina 29634
Email: iwalker@clemson.edu

ABSTRACT

Modeling tendon tensions for applications of tendon-actuated continuum robots under significant loading is necessary for sizing motors, tendons, and other components to ensure that the robot can safely support its mass during operation. While models exist that express tendon tensions as a function of continuum robot configuration, previously proposed models do not consider the effects of gravity on tendon tensions. In this paper, we discuss the addition of gravity to a static model previously developed for low-mass tendon-actuated continuum robots. Using the Euler-Lagrange methodology, the potential energy due to gravity is incorporated into the formulation of the equations that describe tendon tensions as a function of robot configuration. Preliminary experimental results reveal the potential of this nonzero-gravity tendon-tension model.

INTRODUCTION

Continuum 'tongue, trunk and tentacle' robots actively modify the bending along their compliant backbones [1]. This feature allows them to both enter into, maneuver, and operate within tight spaces in which neither conventional rigid-link robots nor people can access, and has made continuum robots the subject of much recent research [2].

This paper is specifically motivated by the application of continuum robots to cement 3D printing applications [3], [4], [5]. In particular, we consider the case when a cement hose is converted into an actively controlled continuum robot [6]. The de-sign concept for 3D printing continuum hoses features tendons routed through specifically designed collars that are placed along the exterior of an industrial cement hose. The continuum robot hose is controlled by actuating motors at the base of the hose. Using a hose as the backbone of a continuum robot would allow for the precise placement of cementious materials with the ability to achieve unique printing orientations and movements not available to previously proposed 3D cement printing methods.

Models which can be used for design optimization are of strong importance for the development of these robots. Modeling tendon tensions during active hose applications of continuum robots is necessary for sizing motors, tendons, and other components to ensure that the robot can safely support its mass during operation. However, compared with previous applications of continuum robots, which have largely been of low-mass and focused on medical procedures [7], external loads, especially gravity, will become a significant factor in operating relatively massive cement-filled continuum backbones. Delivering cement through the hose along the length of the continuum robot adds significant mass that must be supported by the tendons. Few models exist that express tendon tensions as a function of configuration, and previously proposed models do not include the effects of gravity on the tendon tensions [8].

In this paper, we discuss the addition of gravity to a static model previously developed for tendon-actuated continuum robots [8]. The following section discusses the system model and introduces the approach for adding gravity to the model. Results using the model to predict tendon tensions, sup-

ported by preliminary experimental results, are provided and then followed by conclusions.

SYSTEM MODEL

Model Description

We first present the underlying model of a tendon-actuated continuum robot section used herein. The section features three tendons running parallel to the center beam. We assume the beam bends with constant curvature. We define the configuration of the robot using the bending angle θ, the bending plane angle ϕ, and the center beam length L_c [1]. The length of each tendon from the base to their fixed point at the end of the beam is denoted by L_{a_i} ($i = 1, 2, 3$). Fig. 1 identifies these parameters in a diagram showing the tendril robot at some configuration. The tendons run parallel to the center beam in a radially symmetric pattern at a radius R_a from the centerline of the beam, as shown in Fig. 2. The radial angle between each tendon is thus $\frac{2\pi}{3}$ or $120°$.
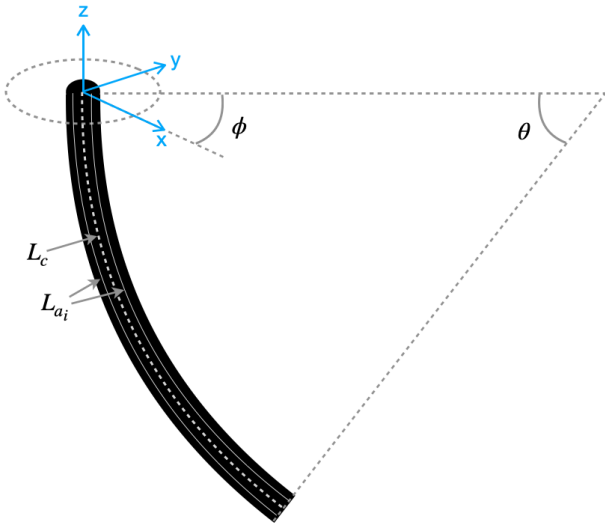

FIGURE 1. SCHEMATIC DIAGRAM OF THE TENDRIL AT SOME CONFIGURATION DEFINED BY θ, ϕ, AND L_{a_i}.

Assumptions for this model match those made in [8] except that herein the effects of gravity are not negligible and that the tendons and the center beam are inextensible. Furthermore, the mass density of the continuum robot is assumed to be uniform such that

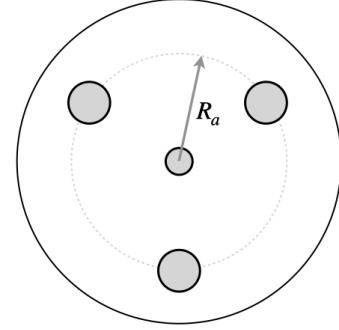$$m(\sigma) = \frac{m}{L_c} \tag{1}$$

FIGURE 2. CROSS-SECTION VIEW OF THE TENDRIL WHERE THE TENDONS RUN THROUGH THE THREE RADIAL HOLES AND THE BACKBONE RUNS THROUGH THE CENTER HOLE.

where m is the total mass of the continuum robot and σ models the arc length along the backbone. With the assumption of constant curvature, the 3-tendon continuum robot is geometrically completely defined by θ, ϕ, and L_c.

Model Derivation

Building on the work in [8], a quasi-static load model is derived from the Euler-Lagrange equations. For the generalized coordinates q, the Euler-Lagrange equations for the continuum robot are given as

$$\frac{\partial V}{\partial q_i} = Q_i \quad i = 1, 2, 3 \tag{2}$$

where V is the potential energy and Q_i is the generalized force for the coordinates $q = [\theta \ \phi \ L_c]^T$. The potential energy considered consists of bending energy (V_b) as defined in [8], and as a new contribution on this paper, the gravitational energy (V_g). Energy due to axial compression in the beam and extension potential energy in the tendons, both considered in [8], is neglected here under the assumption, suitable for the cement hose design, that the tendons and the beam are inextensible.

Beam Bending Potential Energy Using Euler-Bernoulli beam element analysis, the potential energy due to beam bending is given as [9]

$$V_b = \frac{1}{2} \frac{EI}{L_c} \theta^2 \tag{3}$$

where E and I are the Young's modulus and area moment of inertia of the beam.

2

Gravitational Potential Energy   The gravitational potential energy term added to the model in this paper is derived by adapting the methodology described in [10] with the base frame in a different orientation (switching the initial backbone tangent between x and z frames). To simplify the derivation, the curvature of the tendril κ will be introduced and defined as $\kappa = \theta/L_c$. The orientation matrix at σ with respect to the base frame is given by

$$
{}^0\Phi(\sigma) = \begin{bmatrix} \cos(\sigma\kappa(\sigma)) & 0 & -\sin(\sigma\kappa(\sigma)) \\ 0 & 1 & 0 \\ \sin(\sigma\kappa(\sigma)) & 0 & \cos(\sigma\kappa(\sigma)) \end{bmatrix} \tag{4}
$$

The position vector of some point σ along the backbone from the origin with respect to the base frame is evaluated as

$$
{}^0p(\sigma) = \int_0^\sigma {}^0\Phi(\eta)\,[0\ 0\ 1]^T\,d\eta \tag{5}
$$

The potential energy due to gravity at some slice at point σ is given as

$$
V_g(\sigma) = -m(\sigma)\,g^T(\sigma)\,p(\sigma) \tag{6}
$$

where $g^T(\sigma)$ is defined as

$$
g^T(\sigma) = \Phi^T(0)[0\ 0\ -g]^T \tag{7}
$$

and where g is the acceleration due to gravity. Combining Eqns. (1), (5), (6), and (7), the potential energy due to gravity of some slice of mass at point σ along the backbone is evaluated as

$$
V_g(\sigma) = \frac{mg}{L_c\kappa(\sigma)}[\sin(2\sigma\kappa(\sigma)) - \sin(\sigma\kappa(\sigma))] \tag{8}
$$

The total potential energy due to gravity is calculated by integrating over every slice as follows

$$
V_g = \int_0^{L_c} V_g(\sigma)\,d\sigma \tag{9}
$$

Evaluating this integral results in

$$
V_g = \frac{mg}{L_c\kappa^2}\left(\cos(L_c\kappa) - \frac{1}{2}\cos(2L_c\kappa) - \frac{1}{2}\right) \tag{10}
$$

Substituting the general coordinate θ knowing that $\theta = L_c\kappa$ yields

$$
V_g = \frac{mgL_c}{\theta^2}\left(\cos(\theta) - \frac{1}{2}\cos(2\theta) - \frac{1}{2}\right) \tag{11}
$$

Generalized Force   Substituting Eqns. (3) and (11) into (2) yields the generalized forces of the 3-tendon continuum robot as

$$
\begin{aligned}
Q_\theta &= \frac{EI}{L_c} + \frac{mgL_c}{\theta^2}\Big(\frac{1}{\theta}\big(\cos(2\theta) - 2\cos\theta + 1\big) \\
&\quad + \big(\sin(2\theta) - \sin\theta\big)\Big) \\
Q_\phi &= 0 \\
Q_{L_c} &= \frac{mg}{\theta^2}\left(\cos\theta - \frac{1}{2}\cos(2\theta) - \frac{1}{2}\right)
\end{aligned} \tag{12}
$$

These three generalized forces corresponding to the generalized coordinates can also be expressed as [8]

$$
\begin{aligned}
Q_\theta &= \sum_{i=1}^n \left(F_i \frac{\partial L_{a_i}}{\partial \theta}\right) \\
Q_\phi &= \sum_{i=1}^n \left(F_i \frac{\partial L_{a_i}}{\partial \phi}\right) \\
Q_{L_c} &= \sum_{i=1}^n \left(F_i \frac{\partial L_{a_i}}{\partial L_c}\right)
\end{aligned} \tag{13}
$$

where F_i is the tendon tension load in tendon i, and L_{a_i} are the actuator displacements defined in [8] as

$$
L_{a_i} = R_a\theta\cos(\alpha_i),\ \ i = 1,2,3 \tag{14}
$$

and where α_i is defined as

$$
\alpha_i = \phi - 2\pi\frac{i-1}{n},\ \ i = 1,2,3 \tag{15}
$$

3

Combining Eqns. (13) and (14), the generalized forces are given by

$$Q_\theta = R_a \sum_{i=1}^{n} (F_i \cos \alpha_i)$$

$$Q_\phi = R_a \theta \sum_{i=1}^{n} (-F_i \sin \alpha_i) \qquad (16)$$

$$Q_{L_c} = \sum_{i=1}^{n} (F_i)$$

Using Eqns. (12) and (16), the tendon tension loads for each tendon as a function of beam configuration can be derived as

$$
\begin{aligned}
F_i = {} & \frac{mg}{3\theta^2} \left(\cos\theta - \frac{1}{2}\cos(2\theta) - \frac{1}{2} \right) \\
& - \frac{2}{3} \frac{\cos\alpha_i}{R_a} \left\{ \frac{EI}{L_c}\theta + \frac{mgL_c}{\theta^2} \left[\frac{1}{\theta}(\cos(2\theta) - 2\cos\theta + 1) \right. \right. \\
& \left. \left. + (\sin(2\theta) - \sin\theta) \right] \right\}, \quad i = 1,2,3
\end{aligned}
$$

$$(17)$$

EXPERIMENTS
Experimental Methods

To validate that the proposed tendon tension model suitably models the effect of gravity on tendon tensions, tests were performed with a 3-tendon continuum tendril robot [11]. An image of the tendril is shown in Fig. 3.

The center backbone of the tendril is a carbon tube and the tendons are inextensible strings which are threaded through disks attached to the carbon tube, as labeled in Fig. 4. The carbon tube was determined to have a modulus of elasticity E of 94.52 GPa and an area moment of inertia I of 1.67E-12 m^4. The length of the actuated tendril L_c is 933 mm and the radial distance from the centerline of the beam to the tendons R_a is 6.4 mm. The tendons are actuated using three DC motors with encoders and the tension in each tendon is measured using a simple spring mechanism attached to each motor along with a load cell. An Arduino Mega microcontroller is used to send commands to the tendril and to receive data from the load cells on each motor that measure the tendon tensions. The Arduino Mega communicates with a PC computer over Bluetooth. The actuation commands are in the form of encoder counts, with 10500 encoder counts per motor revolution.

FIGURE 3. THE TENDON-DRIVEN CONTINUUM ROBOT USED FOR EXPERIMENTAL TENSION TESTING.

Experimental Procedures

This section on experimental procedures describes the methods that were planned before interruptions to lab work due to COVID-19. Only part of the experimental procedures were completed, and future work aims to complete the data collection to verify the model.

Under the assumption that relative magnitudes of the tendon tensions at different plane angles are the same regardless of gravity or the robot parameters, only the effect of different bending angles on the tendon tensions need be studied experimentally. The robot was configured to achieve a set of increasing bending angles at four different plane angles within the set of plane angles that produces a unique set of results: 0°, 30°, 45°, and 60°. One motor was chosen as the base motor while the actuation of the other motors were determined relative to the base motor depending on the plane angle. For example, for a plane angle of 0° and an angle of rotation for the base motor of 90°, the other motors rotate -45° to add slack to the other two tendons.
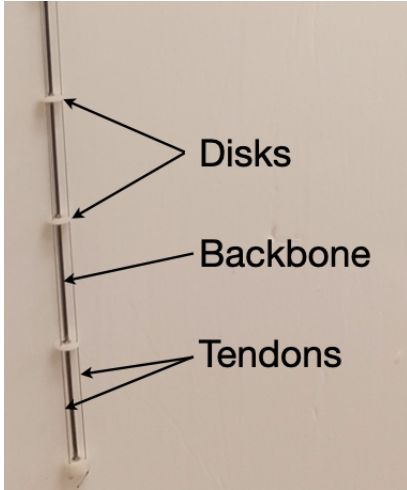
For each plane angle, the robot was actuated to achieve 16

4

FIGURE 4. COMPONENTS OF THE TENDON-DRIVEN CONTINUUM ROBOT USED FOR EXPERIMENTAL TENSION TESTING.

FIGURE 5. THEORETICAL AND EXPERIMENTAL TENDON TENSIONS AT DIFFERENT BENDING ANGLES WITH A CONSTANT PLANE ANGLE OF $175°$.

configurations at different bending angles based on motor revolutions. The length from the base to the tip of the tendril was measured and designated as a chord within the circle traced by part of the tendril. This chord length along with the tendril length L_c (or more appropriately in this case the arc length) was used to calculate the bending angle. The tension of each tendon for each configuration was recorded as well.

Experimental Results

Only a preliminary set of configuration and tension data at a plane angle of $175°$ was recorded. Again, due to the impact of COVID-19, a more complete dataset could not be collected at this time.

For each of the set of configurations recorded in the experimental procedures, the corresponding theoretical tendon tensions were calculated using Eqn. (17). A plot for the preliminary experimental and theoretical tendon-tensions is shown in Fig. 5.

For the data used to generate these plots, any calculated or measured tension values of less than zero are set to zero since negative tension values have no physical meaning. Both plots show that the experimental data generally aligns with the trends of the theoretical results. For Fig. 5, as the bending angle increases, the tendon tensions increase proportionally depending on the plane angle. Qualitatively, the experimental model agrees more with the theoretical model for the bending angles than with the plane angles.

With more data, polynomial fitting of the experimental data and error analysis compared to the theoretical data could be performed. In future work, such a procedure will be employed to quantitatively compare the theoretical model with the experimental results.
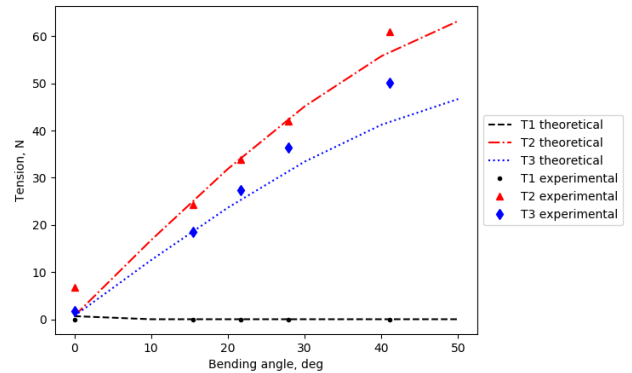
Conclusion

Continuum robots have the potential to significantly expand the functionality and flexibility of previously proposed 3D cement printing methods. Printing cement at large scales through an industrial cement hose converted into a continuum robot could enable the printing of unique shapes and structures. However, transferring cement through a continuum robot hose adds significant mass to the robot, in contrast to previous continuum robot applications in which mostly low-mass continuum robots have been modeled and deployed. Models providing tendon tensions as a function of configuration of tendon-actuated continuum robots exist, but neglect the effect of gravity on the tendon tensions. This paper expands on the tendon-tension model developed in [8] by incorporating the potential energy of gravity into the Euler-Lagrange derivation of the model. The result is a model providing the tendon-tensions of a 3-tendon continuum robot section as a function of robot configuration incorporating gravity. Preliminary experimental data presented herein generally follow the trend of the theoretical model. Future work using more extensive tendon-tension data and a refined experimental setup will further validate the model and provide more quantitative support for the analysis. With a robust tendon-tension model, motors, tendons, and other components of continuum robot hose systems can be sized appropriately to ensure that the system can safely support and control the large mass of cement or other similar fluids for 3D printing applications.

Acknowledgements

5

REFERENCES

[1] R.J. Webster, I., and Jones, B., 2010. "Design and kinematic modeling of constant curvature continuum robots: A review". *International Journal of Robotics Research, 29*, pp. 1661–1683.

[2] D. Trivedi, C.D. Rahn, W. K., and Walker, I., 2008. "Soft robotics: Biological inspiration, state of the art, and future research". *Applied Bionics and Biomechanics, 5*, pp. 99–117.

[3] B. Khoshnevis, D. Hwang, K.-T. Y., and Yeh, Z., 2006. "Mega-scale fabrication by contour crafting". *International Journal of Industrial and Systems Engineering, 1*, pp. 301–320.

[4] C. Gosselin, R. Duballet, P. R. N. G. J. D., and Morel, P., 2016. "Large-scale 3d printing of ultra-high performance concrete – a new processing route for architects and builders". *Mater. Des, 100*, p. 102–109.

[5] Sakin, M., and Kiroglu, Y., 2017. "3d printing of buildings: Construction of the sustainable houses of the future by bim". *Energy Procedia, 134*, pp. 702–711.

[6] Walker, I., and Leonard, E., 2020. "Continuum robot cables and hoses for adaptive inspection and pumping". *International Journal of Technology and Engineering Studies, 5*.

[7] J. Burgner-Kars, D. R., and Choset, H., 2015. "Continuum robots for medical applications: A survey". *IEEE Transactions on Robotics, 31*, pp. 1261–1280.

[8] Dalvand, M. M., Nahavandi, S., and Howe, R. D., 2018. "An analytical loading model for *n*-tendon continuum robots". *IEEE Transactions on Robotics, 34*(5), pp. 1215–1225.

[9] Shabana, A. A., 2008. *Computational Continuum Mechanics*. Cambridge University Press.

[10] Tatlicioglu, E., Walker, I. D., and Dawson, D. M., 2007. "New dynamic models for planar extensible continuum robot manipulators". In 2007 IEEE/RSJ International Conference on Intelligent Robots and Systems, pp. 1485–1490.

[11] M.M. Tonapi, I.S. Godage, A. V., and Walker, I., 2015. "A novel continuum robotic cable aimed at applications in space". *Advanced Robotics, 29*, pp. 861–875.